DOI: 10.1111/mice.12953

RESEARCH ARTICLE

COMPUTER-AIDED CIVIL AND INFRASTRUCTURE ENGINEERING WILEY

A dynamically bi-orthogonal solution method for a stochastic Lighthill-Whitham-Richards traffic flow model

Tianxiang Fan[1] | **S. C. Wong**[1,2] | **Zhiwen Zhang**[3] | **Jie Du**[4,5]

[1]Department of Civil Engineering, The University of Hong Kong, Pok Fu Lam, Hong Kong SAR, China

[2]Guangdong–Hong Kong–Macau Joint Laboratory for Smart Cities, Hong Kong SAR, China

[3]Department of Mathematics, The University of Hong Kong, Pok Fu Lam, Hong Kong SAR, China

[4]Yau Mathematical Sciences Center, Tsinghua University, Beijing, China

[5]Yanqi Lake Beijing Institute of Mathematical Sciences and Applications, Beijing, P. R. China

Correspondence
S. C. Wong, Department of Civil Engineering, The University of Hong Kong, Pok Fu Lam, Hong Kong SAR, China.
Email: hhecwsc@hku.hk

Funding information
Postgraduate Scholarship from the University of Hong Kong; Research Grants Council of the Hong Kong Special Administrative Region, China, Grant/Award Numbers: 17204919, R5029-18, 17300318, 17307921; Francis S Y Bong Professorship in Engineering; National Natural Science Foundation of China, Grant/Award Number: NSFC 11801302; Tsinghua University Initiative Scientific Research Program

Abstract

Macroscopic traffic flow modeling is essential for describing and forecasting the characteristics of traffic flow. However, the classic Lighthill–Whitham–Richards (LWR) model only provides equilibrium values for steady-state conditions and fails to capture common stochastic variabilities, which are a necessary component of accurate modeling of real-time traffic management and control. In this paper, a stochastic LWR (SLWR) model that randomizes free-flow speed is developed to account for the stochasticity incurred by the heterogeneity of drivers, while holding individual drivers' behavior constant. The SLWR model follows a conservation law of stochastic traffic density and flow and is formulated as a time-dependent stochastic partial differential equation. The model is solved using a dynamically bi-orthogonal (DyBO) method based on a spatial basis and stochastic basis. Various scenarios are simulated and compared with the Monte Carlo (MC) method, and the results show that the SLWR model can effectively describe dynamic traffic evolutions and reproduce some commonly observed traffic phenomena. Furthermore, the DyBO method shows significant computational advantages over the MC method.

1 | INTRODUCTION

Traffic flow modeling is fundamental for describing and predicting the characteristics of vehicular movements, and it is an important component of dynamic traffic assignment and real-time traffic management and control. At the macroscopic level, traffic flow modeling focuses on the dynamic changes in flow, density, and speed, as well as shock formation and propagation, with the Lighthill–Whitham–Richards (LWR) model being a classic and

popular model (Lighthill & Whitham, 1955; Richards, 1956). The LWR model is a time-dependent deterministic partial differential equation (PDE) that obeys a conservation law of traffic density and flow. However, it ignores stochastic variabilities, which are common because of differences in driving behavior, vehicle types, and road conditions. The LWR model must be extended to capture these stochastic variabilities in traffic flow. However, stochastic modeling increases the computational burden, so an efficient solution method must be developed to improve its applicability in engineering practice.

Stochastic phenomena are commonly observed in daily traffic (Sumalee et al., 2011; Szeto et al., 2011; Zhou et al., 2016). For example, commuting time can vary on a fixed route across different weekdays even when the average travel time is stable. Therefore, it is unrealistic to assume that traffic dynamics are consistent across days, even at the same location, with the same traffic demands. Considerable effort has been made to explore stochasticity including macroscopic, mesoscopic, and microscopic modeling (Adeli & Ghosh-Dastidar, 2004; Ghosh-Dastidar & Adeli, 2006; Martínez & Jin, 2020). In macroscopic traffic flow modeling, the LWR model offers simplicity and powerful explanations of shock formation and propagation. However, it describes traffic dynamics as a temporal phenomenon (Prigogine & Herman, 1971). To examine how stochasticity can affect the traffic flow, it is necessary to recognize that randomness can come from exogenous sources such as traffic, road geometry design features, and weather conditions or from endogenous sources such as driving behavior (Sumalee et al., 2011). Studies have suggested three strategies to evaluate these uncertainties. One strategy is to randomize the density function. Sumalee et al. (2011) proposed a stochastic cell transmission model (CTM) with a zero-mean Gaussian random process to form a probabilistic density. Randomizing the speed function can also be effective. Li et al. (2012) modified the speed–density function by including a random noise term and then developed an extended LWR model based on these random fundamental relationships. Another option is to randomize the flow function. Jabari and Liu (2012) developed a CTM-based stochastic model using random state-dependent vehicle time headways. They also argued that adding random noise terms to a deterministic equation, which was once a common way to model stochastic traffic flow, can lead to negative densities and mean dynamics, which are inconsistent with those in deterministic dynamics (Gazis & Knapp, 1971; Gazis & Liu, 2003). These studies did not clearly state what governs the stochasticity, and the random noise terms may not reveal consistent factors. For example, driving behavior may be shaped by drivers' memories or tendencies (Cassidy & Windover, 1995). To extend the research into stochastic traffic flow modeling, this paper proposes a new framework for examining the stochasticity stemming from driver heterogeneity, while holding individual drivers' behavior constant. Consequently, a random free-flow speed is introduced into the LWR model and a stochastic PDE (SPDE) is constructed.

Despite the abundant research on solving SPDEs, it remains challenging to balance accuracy and efficiency. The classic Monte Carlo (MC) method is a robust technique to calculate stochastic solutions, with desirable features including the independence of the convergence rate from stochastic dimensionality and the parallelizability of computation (Cheng et al., 2013a, 2013b). However, a disadvantage of the MC method is its slow convergence. MC-based methods with improved sampling techniques have been developed, such as the sparse grid-based stochastic collocation method (Babuška et al., 2007), the multi-level MC method (Giles, 2008), and the internal MC method (Jahani et al., 2014). Jahani et al. (2014) modeled uncertain variables as fuzzy random variables and evaluated them using interval MC simulations and the interval finite element method. These methods, which can be categorized as statistical methods, are not suitable when there is a large number of random variables. Many studies have examined non-statistical methods such as moment equations, perturbation-based methods, and spectral methods (Wan & Karniadakis, 2006; Xiu & Em Karniadakis, 2003; Xiu et al., 2002). However, the number of basis functions in generalized polynomial chaos increases exponentially and makes this approach inefficient for high-dimensional problems. Motivated by the fact that many high-dimensional SPDE problems have certain low-dimensional structures, reduced-complexity models that retain as much of the original predictive capability as possible, such as the Karhunen–Loeve (KL) expansion or the Wiener–Askey polynomial chaos expansion, have been studied. Newman (1996a, 1996b) used the KL expansion and Galerkin's method to find reduced-complexity models for flow-involved dynamical systems. Xiu and Em Karniadakis (2003) proposed a Wiener–Askey polynomial chaos expansion to represent stochastic processes and demonstrated an exponential convergence rate by solving a stochastic ordinary differential equation (ODE). However, these methods require the formation of covariance matrices and the solving of large-scale eigenvalue problems, both of which are computationally expensive. To solve this problem, researchers have studied a dynamically bi-orthogonal (DyBO) method (Babaee et al., 2017; Cheng et al., 2013a, 2013b; Choi et al., 2014) that derives an equivalent system to govern the evolution of the spatial basis and stochastic basis in the KL expansion. This method can be used to construct a reduced basis on the fly without the need to form a covariance matrix or compute

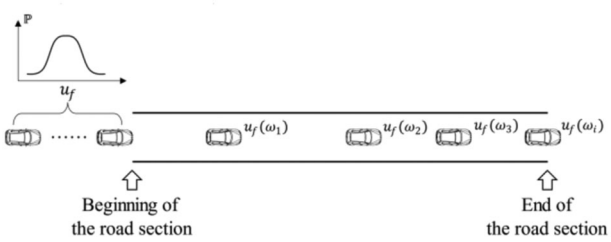

FIGURE 1 Conceptual diagram of the stochastic Lighthill–Whitham–Richards (SLWR) model

its eigendecomposition, which can be much more competitive with high-dimensionality problems. To the best of our knowledge, such a method has never been applied to macroscopic stochastic traffic flow modeling. Due to the high non-linearity in the proposed model, it is challenging to examine its applicability.

Motivated by previous studies of stochastic traffic flow modeling and solution methods, the objectives of this paper are as follows:

1. To propose a new framework for examining the heterogeneity of drivers while holding individual drivers' behavior consistent; specifically, the free-flow speed is randomized in a stochastic LWR (SLWR) model.
2. To apply a highly efficient solution method, that is, the DyBO method, to enhance the applicability of the SLWR model.

To validate the model's properties and the feasibility of the solution method, two simulation experiments that consider temporal bottleneck and geometric bottleneck were conducted, and the MC method was used to obtain benchmark results for comparison.

2 | STOCHASTIC TRAFFIC FLOW MODEL

In macroscopic modeling, traffic flow is described as a continuous fluid, and the distribution, evolution, and propagation of density, speed, and flow are studied. A homogeneous highway road section without any entries or exits is assumed, where all of the vehicles enter at the beginning of the road section and travel to the end of the road section (see Figure 1).

The rationale of the SLWR model is as follows.

1. The stochasticity is assumed to stem from the heterogeneity of drivers.
2. The heterogeneity is reflected in free-flow speed, which represents the different desired speed choices on an empty or perceived empty road.
3. The free-flow speed can be regarded as an endogenous driving behavior that is potentially related to a driver's personality.

Therefore, it is reasonable to assume that the free-flow speed of a single driver does not vary across time and space. For example, conservative drivers travel more slowly than aggressive drivers in the free-flow condition, and a driver is unlikely to keep switching from conservative to aggressive driving behaviors across a road section within a short period.

In this paper, let u_f be the free-flow speed, which is a random parameter that could follow any type of distribution, defined on a probability space $(\Omega, F, \mathbb{P})$, representing heterogeneous driving behavior.

$$u_f : \Omega \to \mathbb{R} \tag{1}$$

where Ω is a sample space, F is a σ-algebra, $\mathbb{P}$ is a probability measure, and $\mathbb{R}$ is a real line. Then, $u_f(\omega)$ is the random free-flow speed that corresponds to the random event $\omega \in \Omega$.

At the beginning of the road section, traffic flow is a stochastic process defined on the same probability space:

$$\{Q_{in}(t,\omega) : t \in [0,T], \omega \in \Omega\} \tag{2}$$

where $Q_{in}(t,\omega)$ is the traffic flow at the beginning of the road section, and t represents the evolving time from 0 to T. Therefore, every $t \in [0,T]$ corresponds to some random variable $Q_{in}(t,\cdot) : \Omega \to \mathbb{R}$, which indicates that traffic flow at the beginning of the road section can randomly change over time.

In combination with the definitional relationship and Greenshields's model, the traffic dynamics of any certain driver can be described by:

$$q\left(x,t,u_f(\omega)\right) = k\left(x,t,u_f(\omega)\right) u\left(x,t,u_f(\omega)\right) \tag{3}$$

$$u\left(x,t,u_f(\omega)\right) = u_f(\omega) - \frac{u_f(\omega)}{k_{jam}} k\left(x,t,u_f(\omega)\right) \tag{4}$$

where $q(x,t,u_f(\omega))$ is the traffic flow; $k(x,t,u_f(\omega))$ is the traffic density; $u(x,t,u_f(\omega))$ is the traffic speed; and k_{jam} is the jam density. These show that for a given free-flow speed, traffic dynamics are non-random variables across the highway section over time.

In light of fluid mechanics, vehicular movements through the assumed road section can be described in terms of the conservation law, so the general specification of the SLWR model can be described as

follows:

$$\frac{\partial k\left(x,t,u_f(\omega)\right)}{\partial t}+\frac{\partial q\left(x,t,u_f(\omega)\right)}{\partial x}=0,\ x\in[a,b],\ t\in[0,T],\omega\in\Omega \tag{5}$$

$$k\left(x,0,u_f(\omega)\right)=k_0\left(x,u_f(\omega)\right) \tag{6}$$

$$q\left(a,t,u_f(\omega)\right)=Q_{in}\left(t,\omega\right) \tag{7}$$

where x represents the spatial dimension, that is, the length of the road section from point a to point b; Equation (5) is the conservation law, Equation (6) shows the initial condition, and Equation (7) shows the boundary condition.

The proposed model indicates that the boundary condition will evolve randomly with time, but once the free-flow speed is sampled, its corresponding traffic dynamics will obey the conservation law. This means that randomness only enters the system through the boundary condition because of heterogeneous drivers, which satisfies our assumptions.

As the time-varying compositions of drivers are randomly generated at the beginning of a road section, stochasticity exists at every time and location. In other words, the free-flow speed is considered a random parameter, but it does not only reflect the randomness at the free-flow state. For example, given a specific density k, traffic flow and time headway are also random variables with the means and variances as follows:

$$E\left(q\right)=\bar{u}_f\left(k-\frac{k^2}{k_j}\right) \tag{8}$$

$$Var\left(q\right)=k^2\left(1-\frac{k}{k_j}\right)^2\sigma_{u_f}^2 \tag{9}$$

$$E\left(\tau\right)=\frac{1}{\bar{u}_f}\left(k-\frac{k^2}{k_j}\right)^{-1}+\frac{1}{\bar{u}_f^3}\left(k-\frac{k^2}{k_j}\right)^{-1}\sigma_{uf}^2 \tag{10}$$

$$Var\left(\tau\right)=\frac{1}{\bar{u}_f^4}\left(k-\frac{k^2}{k_j}\right)^{-2}\sigma_{uf}^2-\frac{1}{\bar{u}_f^6}\left(k-\frac{k^2}{k_j}\right)^{-2}\sigma_{u_f}^4 \tag{11}$$

where $E(q)$ is the mean of traffic flow, $Var(q)$ is the variance of traffic flow, $E(\tau)$ is the mean of time headway, $Var(\tau)$ is the variance of time headway, $\bar{u}_f$ is the mean of free-flow speed, and $\sigma_{u_f}^2$ is the variance of free-flow speed.

3 | SOLUTION METHODS

To numerically solve the SLWR model, the DyBO method was first adopted to transform the SPDE into a series of deterministic PDEs and ODEs. Classic finite difference methods can then be applied. The fifth-order weighted essentially non-oscillatory (WENO5) scheme was used.

3.1 | DyBO solution method

The derivation of the DyBO formulation of the SLWR model is presented below. Combining Equations (3)–(5), the SLWR model can be written as

$$\frac{\partial k\left(x,t,u_f(\omega)\right)}{\partial t}=\mathcal{L}k=\left(2\frac{u_f(\omega)}{k_{jam}}k\left(x,t,u_f(\omega)\right)-u_f(\omega)\right)\frac{\partial k\left(x,t,u_f(\omega)\right)}{\partial x} \tag{12}$$

where $\mathcal{L}$ is a differential operator, and k_{jam} is the jam density (a constant value).

According to the KL expansion (Newman, 1996a, 1996b), denoted by $\tilde{k}$ the m-term truncated solution of Equation (12):

$$\tilde{k}=\bar{k}+\boldsymbol{k}\boldsymbol{Y}^T \tag{13}$$

$$\boldsymbol{k}\left(x,t\right)=\left(k_1\left(x,t\right),k_2\left(x,t\right),\ldots,k_m\left(x,t\right)\right) \tag{14}$$

$$\boldsymbol{Y}\left(\omega,t\right)=\left(Y_1\left(\omega,t\right),Y_2\left(\omega,t\right),\ldots,Y_m\left(\omega,t\right)\right) \tag{15}$$

$$Cov_k\left(x,y\right)=E\left[\left(k\left(x,t,u_f(\omega)\right)-\bar{k}\left(x,t\right)\right)\left(k\left(y,t,u_f(\omega)\right)-\bar{k}\left(y,t\right)\right)\right] \tag{16}$$

where $\bar{k}=E[\tilde{k}]$, $\boldsymbol{k}(x,t)$ is the spatial basis, that is, a vector of eigenfunctions of the associated covariance function of Equation (16); $\boldsymbol{Y}(\omega,t)$ is the stochastic basis, that is, a vector of zero-mean random variables; and m is the number of truncated terms. Correspondingly, $<\boldsymbol{k}^T,\boldsymbol{k}>$ and $E[\boldsymbol{Y}^T\boldsymbol{Y}]$ are m-by-m matrices and satisfy the bi-orthogonality condition as

$$<\boldsymbol{k}^T,\boldsymbol{k}>\left(t\right)=\left(<k_i,k_j>\right)=\left(\lambda_i\left(t\right)\delta_{ij}\right)_{m\times m} \tag{17}$$

$$E\left[\boldsymbol{Y}^T\boldsymbol{Y}\right]\left(t\right)=\left(E\left[Y_iY_j\right]\right)=\boldsymbol{I} \tag{18}$$

where $\lambda_i(t)$ is the corresponding eigenvalues of the covariance function of Equation (16), δ_{ij} is the Kronecker product, and $\boldsymbol{I}$ is the identity matrix.

Substitute Equation (13) into Equation (12),

$$\frac{\partial\bar{k}}{\partial t}+\frac{\partial\boldsymbol{k}}{\partial t}\boldsymbol{Y}^T+\boldsymbol{k}\frac{d\boldsymbol{Y}^T}{dt}=\mathcal{L}\tilde{k}+\left\{\mathcal{L}k-\mathcal{L}\tilde{k}\right\}-\left\{\frac{\partial\tilde{\boldsymbol{k}}}{\partial t}\tilde{\boldsymbol{Y}}^T+\tilde{\boldsymbol{k}}\frac{d\tilde{\boldsymbol{Y}}^T}{dt}\right\} \tag{19}$$

and assume that the eigenvalues in the KL expansion decay fast enough and the differential operator is stable; then, the last two terms on the right-hand side will be small and can be dropped.

$$\frac{\partial \bar{k}}{\partial t} + \frac{\partial \boldsymbol{k}}{\partial t}\boldsymbol{Y}^T + \boldsymbol{k}\frac{d\boldsymbol{Y}^T}{dt} = \mathcal{L}\tilde{k} \tag{20}$$

Take expectations on both sides of Equation (19), and because $\boldsymbol{Y}$ is a zero-mean random variable,

$$\frac{\partial \bar{k}}{\partial t} = E\left[\mathcal{L}\tilde{k}\right] \tag{21}$$

which gives the evolution equation for the mean of the solution.

Multiplying both sides of Equation (20) by $\boldsymbol{Y}$ from the right and taking expectations, the evolution equation of the spatial basis can be obtained. Similarly, multiplying both sides of Equation (20) by $\boldsymbol{k}$ from the right, the evolution equation of the stochastic basis can be obtained. More detailed steps of the derivation can be found in Cheng et al. (2013a, 2013b).

$$\frac{\partial \boldsymbol{k}}{\partial t} = -\boldsymbol{k}\boldsymbol{D}^T + E\left[\tilde{\mathcal{L}}\tilde{k}\boldsymbol{Y}\right] \tag{22}$$

$$\frac{d\boldsymbol{Y}}{dt} = -\boldsymbol{Y}\boldsymbol{C}^T + < \tilde{\mathcal{L}}\tilde{k}, \boldsymbol{k} > \boldsymbol{\Lambda}_{\boldsymbol{k}}^{-1} \tag{23}$$

where $\boldsymbol{C}$ and $\boldsymbol{D}$ are m-by-m matrices representing the projection coefficients of $\frac{\partial \boldsymbol{k}}{\partial t}$ and $\frac{d\boldsymbol{Y}}{dt}$ into $\boldsymbol{k}$ and $\boldsymbol{Y}$, respectively. The solutions of $\boldsymbol{C}$ and $\boldsymbol{D}$ are given entry-wisely:

$$C_{ii} = G_{*ii} \tag{24}$$

$$C_{ij} = \frac{\|k_j\|^2}{\|k_j\|^2 - \|k_i\|^2}\left(G_{*ij} + G_{*ji}\right), \text{ for } i \neq j \tag{25}$$

$$D_{ii} = 0 \tag{26}$$

$$D_{ij} = \frac{1}{\|k_j\|^2 - \|k_i\|^2}\left(\|k_j\|^2 G_{*ji} + \|k_i\|^2 G_{*ij}\right), \text{ for } i \neq j \tag{27}$$

where C_{ii}, C_{ij} are elements of the matrix $\boldsymbol{C}$; D_{ii}, D_{ij} are elements of the matrix $\boldsymbol{D}$; and G_{*ij}, G_{*ji} are elements of the matrix $\boldsymbol{G}_*$, which can be calculated as

$$\boldsymbol{G}_* = \boldsymbol{\Lambda}_{\boldsymbol{k}}^{-1} < \boldsymbol{k}^T, E\left[\tilde{\mathcal{L}}\tilde{k}\boldsymbol{Y}\right] > \tag{28}$$

$$\boldsymbol{\Lambda}_{\boldsymbol{k}} = diag\left(< \boldsymbol{k}^T, \boldsymbol{k} >\right) \tag{29}$$

Equations (22) and (23) still involve random variables. Because the random free-flow speed is assumed to follow a normal distribution in this paper, Hermite polynomials can be used to represent the stochastic terms.

Denote by $\boldsymbol{H} = (H_1, H_2, \ldots, H_{N_p})$ the N_p-term Hermite polynomials, which exclude the zero-index $\boldsymbol{H}_0 = 1$. Then,

$$\boldsymbol{Y} = \boldsymbol{H}\boldsymbol{A} \tag{30}$$

where $\boldsymbol{A}$ is a N_p-by-m matrix.

Denote by $Z_{u_f} = \boldsymbol{c}\boldsymbol{H}^T$ a standard normal (i.e., $Z_{u_f} \sim N(0,1)$), where $\boldsymbol{c} = (1, 0, \ldots, 0)$ is the expansion constants; then, the free-flow speed can be represented as

$$u_f(\omega) = \overline{u_f} + \sigma_{u_f}\boldsymbol{c}\boldsymbol{H}^T \tag{31}$$

where $\overline{u_f}$ is the mean and σ_{u_f} is the standard deviation of the random free-flow speed.

Substituting Equations (13), (30), and (31) into Equation (12),

$$\begin{aligned}\mathcal{L}\tilde{k} = &\left(2\frac{u_f(\omega)}{k_{jam}}\bar{k} - u_f(\omega)\right)\frac{\partial \bar{k}}{\partial x} + \left(\frac{2\bar{k}}{k_{jam}} - 1\right)\overline{u_f}\boldsymbol{H}\boldsymbol{A}\frac{\partial \boldsymbol{k}^T}{\partial x} \\ &+ \left(\frac{2\bar{k}}{k_{jam}} - 1\right)\sigma_{u_f}\boldsymbol{c}\boldsymbol{H}^T\boldsymbol{H}\boldsymbol{A}\frac{\partial \boldsymbol{k}^T}{\partial x} + \frac{2}{k_{jam}}\frac{\partial \bar{k}}{\partial x}\overline{u_f}\boldsymbol{H}\boldsymbol{A}\boldsymbol{k}^T \\ &+ \frac{2}{k_{jam}}\frac{\partial \bar{k}}{\partial x}\sigma_{u_f}\boldsymbol{c}\boldsymbol{H}^T\boldsymbol{H}\boldsymbol{A}\boldsymbol{k}^T + \frac{2}{k_{jam}}\overline{u_f}\boldsymbol{k}\boldsymbol{A}^T\boldsymbol{H}^T\boldsymbol{H}\boldsymbol{A}\frac{\partial \boldsymbol{k}^T}{\partial x} \\ &+ \frac{2}{k_{jam}}\sigma_{u_f}\boldsymbol{c}\boldsymbol{H}^T\boldsymbol{k}\boldsymbol{A}^T\boldsymbol{H}^T\boldsymbol{H}\boldsymbol{A}\frac{\partial \boldsymbol{k}^T}{\partial x}\end{aligned} \tag{32}$$

Then, the following terms $E[\mathcal{L}\tilde{k}]$, $E[\tilde{\mathcal{L}}\tilde{k}\boldsymbol{H}]\boldsymbol{A} = E[(\mathcal{L}\tilde{k} - E[\mathcal{L}\tilde{k}])\boldsymbol{H}]\boldsymbol{A}, E[\boldsymbol{H}^T\tilde{\mathcal{L}}\tilde{k}]$ can be calculated using the properties $E[\boldsymbol{H}^T\boldsymbol{H}] = \boldsymbol{I}, \boldsymbol{A}^T\boldsymbol{A} = \boldsymbol{I}$, and $E[\boldsymbol{H}] = 0$.

Based on the representation of Hermite polynomials, the DyBO formulation of the SLWR model can be expressed as

$$\frac{\partial \bar{k}}{\partial t} = E\left[\mathcal{L}\tilde{k}\right] \tag{33}$$

$$\frac{\partial \boldsymbol{k}}{\partial t} = -\boldsymbol{k}\boldsymbol{D}^T + E\left[\tilde{\mathcal{L}}\tilde{k}\boldsymbol{H}\right]\boldsymbol{A} \tag{34}$$

$$\frac{d\boldsymbol{A}}{dt} = -\boldsymbol{A}\boldsymbol{C}^T + < E\left[\boldsymbol{H}^T\tilde{\mathcal{L}}\tilde{k}\right], \boldsymbol{k} > \boldsymbol{\Lambda}_{\boldsymbol{k}}^{-1} \tag{35}$$

which gives the deterministic PDE of Equations (33) and (34) and ODE of Equation (35).

3.2 | Weighted essentially non-oscillatory scheme

For hyperbolic problems, the solution may contain strong discontinuities even if the initial data are smooth. When dealing with discontinuous solutions, high-order linear schemes generate numerical oscillations. To avoid this problem, non-linear schemes or limiters are needed. This study used the fifth-order WENO5 scheme, which has high resolution and is non-oscillatory even in the presence of shocks and other discontinuities in the solution (Jiang & Shu, 1996; Xiong et al., 2011). More details can be found in Shu (2006, 2020). The procedure of the WENO scheme is summarized below. Consider Equation (33) as an example.

First, spatial discretization is discussed. The space domain is discretized into a uniform mesh of J grid points:

$$x_j = j\Delta x,\ j = 1, 2, \ldots, J \tag{36}$$

where Δx is the uniform grid mesh. Then, the approximation of density $\bar{k}_j(t) \approx \bar{k}(x_j, t)$ satisfies the following equation:

$$\frac{d\bar{k}_j(t)}{dt} + \frac{1}{\Delta x}\left(\hat{q}_{j+\frac{1}{2}} - \hat{q}_{j-\frac{1}{2}}\right) = 0 \tag{37}$$

where $\hat{q}_{j+\frac{1}{2}}$ and $\hat{q}_{j-\frac{1}{2}}$ are the numerical fluxes at points $j + 1/2$ and $j - 1/2$ of the right-hand side of Equation (32), respectively. According to the fifth-order WENO scheme, the numerical flux $\hat{q}_{j+\frac{1}{2}}$ is defined as follows:

$$\hat{q}_{j+\frac{1}{2}} = \theta_1 \hat{q}^{(1)}_{j+1/2} + \theta_2 \hat{q}^{(2)}_{j+1/2} + \theta_3 \hat{q}^{(3)}_{j+1/2} \tag{38}$$

where θ_1, θ_2, and θ_3 are three non-linear weights and $\hat{q}^{(1)}_{j+1/2}$, $\hat{q}^{(2)}_{j+1/2}$, and $\hat{q}^{(3)}_{j+1/2}$ are three third-order numerical fluxes on three stencils. The third-order fluxes are given by:

$$\hat{q}^{(1)}_{j+1/2} = \frac{1}{3} q_{j-2} - \frac{7}{6} q_{j-1} + \frac{11}{6} q_j \tag{39}$$

$$\hat{q}^{(2)}_{j+1/2} = -\frac{1}{6} q_{j-1} + \frac{5}{6} q_j + \frac{1}{3} q_{j+1} \tag{40}$$

$$\hat{q}^{(3)}_{j+1/2} = \frac{1}{3} q_j + \frac{5}{6} q_{j+1} - \frac{1}{6} q_{j+2} \tag{41}$$

where q_j is an abbreviated notation for $q(x_j, t)$. The non-linear weights are given by:

$$\theta_p = \frac{\tilde{\theta}_p}{\sum_{l=1}^{3} \tilde{\theta}_l},\ p = 1, 2, 3 \tag{42}$$

$$\tilde{\theta}_l = \frac{\gamma_l}{(\varepsilon + \beta_l)^2},\ l = 1, 2, 3 \tag{43}$$

where ε is a parameter to prevent the denominator of $\tilde{\theta}_l$ from being zero and is fixed at 10^{-6} in this paper, γ_l is the linear weights, and β_l is the smoothness indicator. The linear weights are given by:

$$\gamma_1 = \frac{1}{10},\ \gamma_2 = \frac{3}{5},\ \gamma_3 = \frac{3}{10} \tag{44}$$

and the smoothness indicators are given by:

$$\beta_1 = \frac{13}{12}\left(q_{j-2} - 2q_{j-1} + q_j\right)^2 + \frac{1}{4}\left(q_{j-2} - 4q_{j-1} + 3q_j\right)^2 \tag{45}$$

$$\beta_2 = \frac{13}{12}\left(q_{j-1} - 2q_j + q_{j+1}\right)^2 + \frac{1}{4}\left(q_{j-1} - q_{j+1}\right)^2 \tag{46}$$

$$\beta_3 = \frac{13}{12}\left(q_j - 2q_{j+1} + q_{j+2}\right)^2 + \frac{1}{4}\left(3q_j - 4q_{j+1} + q_{j+2}\right)^2 \tag{47}$$

Above is described the fifth-order WENO scheme for the positive wind direction. If the wind direction is negative, the procedure for computing the numerical flux $\hat{q}_{j+\frac{1}{2}}$ is a mirror image with respect to the point $x_{j+1/2}$, which is described above. The stencil can then be biased to the right. For the case where the wind direction may change, the Lax–Friedrichs splitting method is used.

$$q\left(\bar{k}\right) = q^+\left(\bar{k}\right) + q^-\left(\bar{k}\right) \tag{48}$$

$$q^{\pm}\left(\bar{k}\right) = \frac{1}{2}\left(q\left(\bar{k}\right) \pm \alpha \bar{k}\right) \tag{49}$$

$$\alpha = \max_k \left|\partial q\left(\bar{k}\right)/\partial \bar{k}\right| \tag{50}$$

where $q^+(\bar{k})$ and $q^-(\bar{k})$ are the splitting flux for the positive and negative wind directions, respectively.

Second, the time domain is discretized into a mesh of N grid points.

$$t^{[n]} = t^{[n-1]} + \Delta t,\ n = 1, 2, \ldots, N \tag{51}$$

where Δt is the uniform mesh size on the time axis. Then, the third-order total variation diminishing Runge–Kutta method is used.

$$\bar{k}^{(1)} = \bar{k}^{[n]} + \Delta t L\left(\bar{k}^{[n]}, t^{[n]}\right) \tag{52}$$

$$\bar{k}^{(2)} = \frac{3}{4}\bar{k}^{[n]} + \frac{1}{4}\bar{k}^{(1)} + \frac{1}{4}\Delta t L\left(\bar{k}^{(1)}, t^{[n]} + \Delta t\right) \tag{53}$$

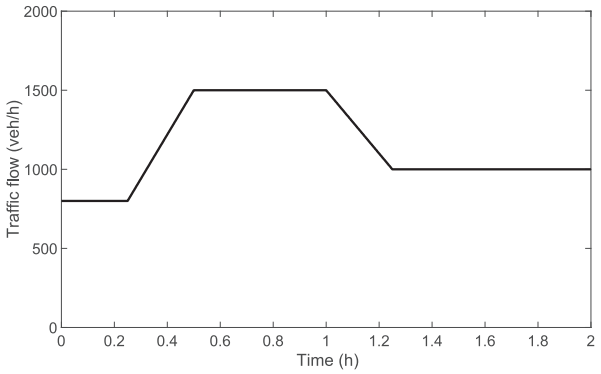

FIGURE 2 Traffic demand at the beginning of the road section

$$\bar{k}^{[n+1]} = \frac{1}{3}\bar{k}^{[n]} + \frac{2}{3}\bar{k}^{(2)} + \frac{2}{3}\Delta t L\left(\bar{k}^{(2)}, t^{[n]} + \frac{1}{2}\Delta t\right) \quad (54)$$

where L is the approximation to the spatial derivatives:

$$L\ (k,t) = -\frac{1}{\Delta x}\left(\hat{q}_{j+\frac{1}{2}} - \hat{q}_{j-\frac{1}{2}}\right) \quad (55)$$

4 | NUMERICAL EXAMPLES

Two simulation experiments were conducted to show the effectiveness of the SLWR model and to demonstrate some commonly observed traffic phenomena. In the first example, a temporal bottleneck was considered. The DyBO method was validated in comparison to the MC method. Different samples of the MC method were calculated to select a benchmark result, and different numbers of spatial terms and Hermite polynomials were tested in the sensitivity analysis. In the second example, more complicated geometric conditions were considered. The SLWR model with the DyBO method still showed excellent performance.

4.1 | Example 1

4.1.1 | Example settings

A 2-km homogeneous highway road section without any intermediate ramps was considered. The free-flow speed was assumed to be a stochastic parameter following a normal distribution with a mean of 70 and a standard deviation of 10, that is, $u_f \sim N(70, 100)$ and $k_{jam} = 100$ veh/km. The initial condition assumed that traffic density was empty along the section, and the boundary condition assumed that traffic flow at the beginning of the road section was subjected to a trapezoid of changes as shown in Figure 2. The simulation period was 1.5 h.

It is assumed that an incident occurs at the end of the road section, fully blocking the road section from $t = 0.75$ h to $t = 0.77$ h. During the blockage period, no vehicles can leave the road section, so a queue emerges and is propagated upstream. After $t = 0.77$ h, the incident is cleared, and the queue discharges. For the WENO5 scheme, the spatial and time grid sizes are set to 0.01 km and 1×10^{-4} h, respectively. This relatively simple example makes it easy for researchers to reproduce the results (Zheng, 2021).

4.1.2 | Numerical results

To validate the DyBO method, a benchmark solution was calculated using the MC method. According to the central limit theorem, as the sample sizes increased, the results of the MC method became closer to the exact values. Samples sizes of 100, 200, 400, 800, 1600, 3200, and 12,800 were calculated, and 12,800 MC samples were computed to approximate the exact solution as a benchmark result. The relative root-mean-squared error (RRMSE) is defined as follows to measure accuracy against the benchmark results.

$$RRMSE_\rho = \frac{\sqrt{\frac{1}{N}\sum_{it}\left(\rho_{it}^{(k)} - \rho_{it}^{*}\right)^2}}{\frac{1}{N}\sum_{it}\rho_{it}^{*}} \times 100\% \quad (56)$$

$$RRMSE_\sigma = \frac{\sqrt{\frac{1}{N}\sum_{it}\left(\sigma_{it}^{(k)} - \sigma_{it}^{*}\right)^2}}{\frac{1}{N}\sum_{it}\sigma_{it}^{*}} \times 100\% \quad (57)$$

where $\rho_{it}^{(k)}$ and $\sigma_{it}^{(k)}$ are the mean (MEAN) and standard deviation (SDEV) of the density of the kth case for grid point (i,t), respectively; ρ_{it}^{*} and σ_{it}^{*} are the converged MEAN and SDEV of the density from the MC scheme, respectively; and N is the total number of grid points (space and time).

Figure 3 shows the RRMSE of the MEAN and SDEV of the density. The MEAN's RRMSE converged faster than that of SDEV. When the sample size was larger than 1600, the MEAN's RRMSE dropped below 0.5%, while the SDEV's RRMSE was approximately 3%.

Although the MC method can obtain robust solutions, its efficiency may be undesirable. As shown in Figure 4, the computation time of the MC method increased linearly, and the case of 12,800 MC samples requires approximately 12,325 min of computing time.

The DyBO method was then applied to reach an acceptable level of accuracy in a much more efficient way. As a blockage incident was considered in the simulation experiment, the results are elaborated in three scenarios: (1) before the blockage, (2) during the blockage, and (3) after the blockage. This can help to clarify the traffic flow propagation. As mentioned, the derivation of DyBO

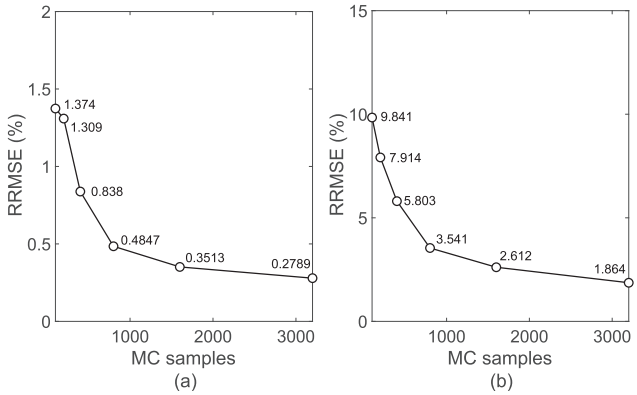

FIGURE 3 Relative root-mean-squared error (RRMSE) of different numbers of MC samples: (a) mean (MEAN) and (b) standard deviation (SDEV)

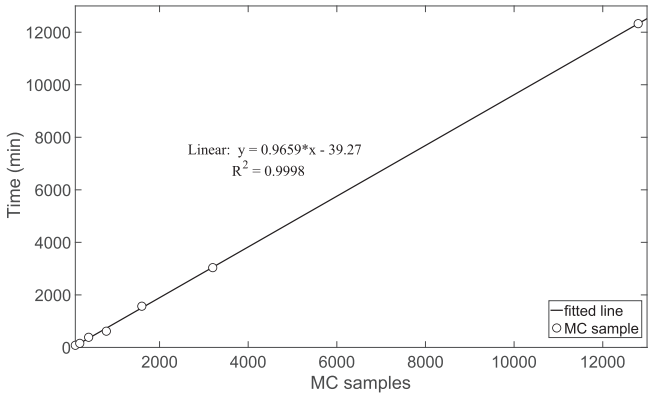

FIGURE 4 Computation time of the Monte Carlo (MC) method

equations involved truncated terms. Therefore, the number of spatial terms or Hermite polynomials can affect the accuracy of the solutions. Different numbers of spatial terms (i.e., $m = 3, 5, 7, 9, 11, 13, 15$) and Hermite polynomials (i.e., $N_p = 2, 4, 6$) were tested to examine the sensitivity of accuracy and efficiency.

Before the blockage, traffic entered the left boundary and exited at the right boundary without any disturbance, and a relatively smooth density pattern was observed. Figure 5 shows the density patterns at $t = 0.3$ h. Slight staircase-shaped fluctuations were observed, as vehicles with different free-flow speeds entered stochastically, and faster vehicles traveled farther than slower ones, causing the density to accumulate at different spots. The greater the speed differences, the greater the fluctuations, in line with the findings of Zhang et al. (2003). Furthermore, with increasing spatial terms and Hermite polynomials, the MEAN and SDEV became closer to the results of the MC method.

During the blockage, traffic continuously entered the left boundary but did not leave at the right boundary. A backward shock wave was observed. Figure 6 shows the density patterns at $t = 0.78$ h. The maximum MEAN was 100 veh/h, which is consistent with the jam density of the proposed Greenshields's model. The MEAN dropped to approximately 50 veh/h after the peak, indicating the saturated discharging flow, which is consistent with the optimal density of the Greenshields's model. Even with the shock wave, the DyBO method showed good convergence to the MC results, and the accuracy can be increased by adding more spatial terms and Hermite polynomials.

After the blockage, the queue was discharged at the right boundary, and similar density patterns to those observed before the blockage were observed. Figure 7 shows the density patterns at $t = 1.2$ h. The MEAN and SDEV were relatively stable alongside the road section, with slight fluctuations because of heterogeneous driving behavior, and were generally larger than those at $t = 0.3$ h because of the increased traffic flow at the left boundary. This implies that the SLWR model and DyBO method can adapt well to different boundary conditions.

To quantify the convergence of the DyBO method, the RRMSE of MEAN and SDEV were calculated, with different numbers of spatial terms ($m = 3, 5, 7, 9, 11, 13, 15$) and Hermite polynomials ($N_p = 2, 4, 6$) with respect to the benchmark solutions obtained by the MC method with 12,800 MC samples as shown in Table 1. As the number of spatial terms or Hermite polynomials increased, the RRMSE of MEAN and SDEV decreased, indicating convergence to the benchmark results. With $m = 15$, the RRMSE of both MEAN and SDEV were below 1%, which was acceptable in comparison to the MC results. Furthermore, the computation time of the DyBO method ranged from 1.7 to 2.1 min, which considerably reduced the computational costs.

One major contribution of this paper is the development of an efficient method to solve the SLWR model. The simulation experiment results showed that the DyBO method was much more efficient than the MC method and had desirable accuracy. The speedup performance of the DyBO method was also calculated. It is well known that the convergence of the MC method satisfies the relationship $E = O(1/\sqrt{K}) = C/\sqrt{K}$, where E is the error, K is the number of MC samples, and C is a constant. Taking the logarithm on both sides, a linear relationship is expected, $lnE = lnC - 1/2\ lnK$. Thus, if a graph of lnE against lnK is plotted, the slope of the best-fitted line can be approximately −0.5. According to the RRMSE and sample size of the MC method in Figure 3, two best-fitted lines were plotted, as shown in Figure 8, from which the num-

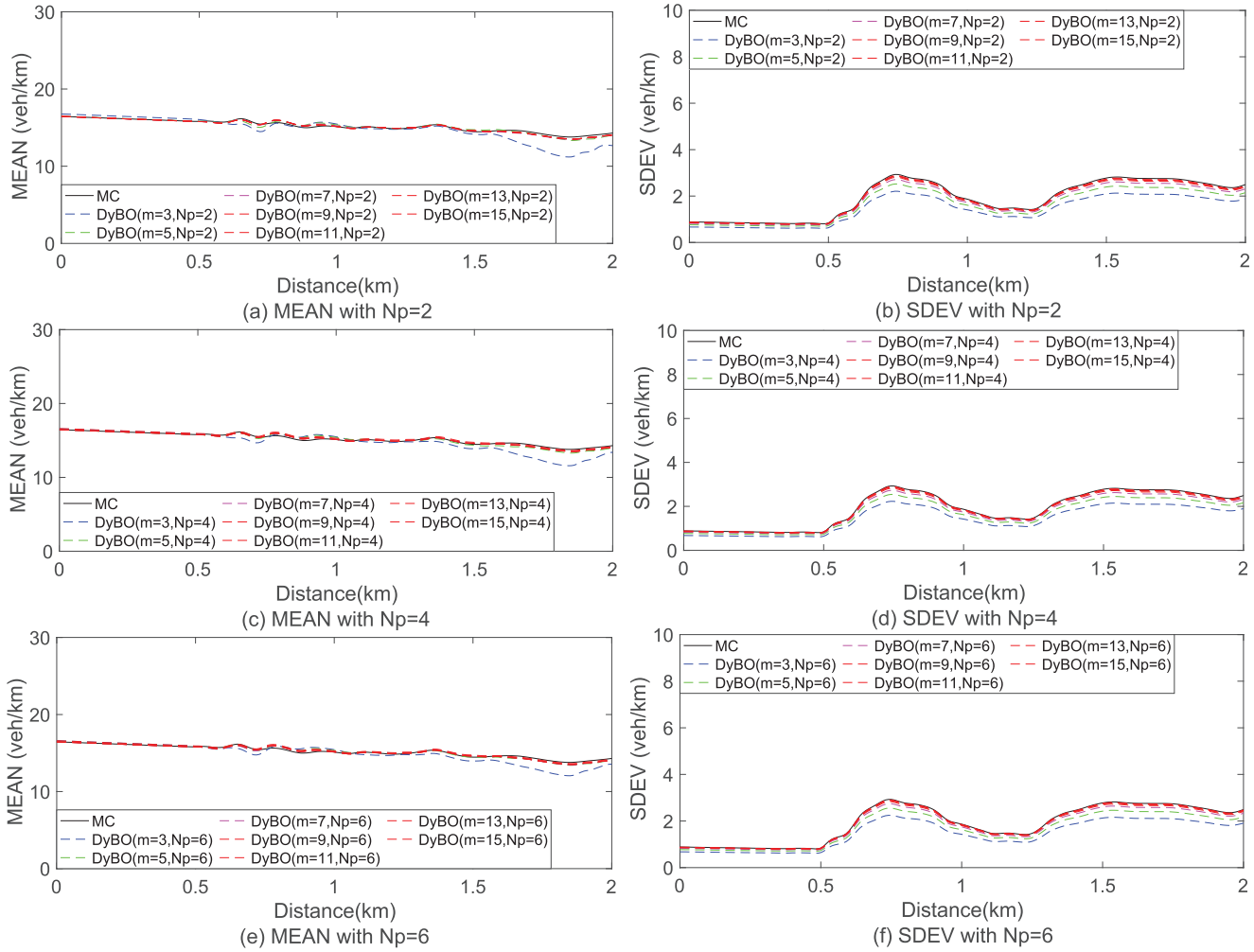

FIGURE 5 Density patterns at $t = 0.3$ h. DyBO, dynamically bi-orthogonal; MC, Monte Carlo; MEAN, mean; SDEV, standard deviation

ber of samples that achieve the same accuracy as the DyBO method can be estimated, and then the speedup can be calculated.

For example, with $m = 15$ and $N_p = 6$, the RRMSE values of MEAN and SDEV were 0.2% and 0.9%, respectively. Based on the best-fitted lines in Figure 8, estimated sample sizes (10,999 and 11,429) can be calculated. To ensure that the accuracy of the DyBO method was not worse than the MC method in terms of both MEAN and SDEV, the smaller sample size of 10,586 was selected, which took approximately 10,586 min using the MC method. The speedup was then calculated as $10586/2.08 \approx 5089$. As calculated, the DyBO method can achieve approximately five to 6000 times speedup over the MC method. As shown in Figure 9, the logarithm of speedup against RRMSE was presented, and it was found that the speedup increased as the RRMSE decreased. With respect to the same RRMSE, the speedup of SDEV was greater than that of MEAN, and with respect to the same speedup, the RRMSE of MEAN was less than that of SDEV. For practical use in engineering problems, the balance between efficiency and accuracy can be assessed. If MEAN is more important and a large error can be tolerated, the MC method will remain popular because of its simplicity; however, if SDEV is of interest and sufficiently small errors are desired, then the DyBO method will be preferable.

As shown in the example 1, the SLWR model can reproduce some commonly observed traffic phenomena. Figure 10 shows that the MEAN of the densities varies with the trapezoidal traffic demand throughout the simulation period; that the densities rapidly increase to the jam density at the beginning of the congestion period and then stabilize due to the bottleneck at the end of the road section. The duration of the completely stopped condition is slightly longer at the 1.75-km location than at the 1.5-km location. A similar phenomenon can be found during the discharging process. This is reasonable, because the shock wave will decrease in the upstream direction once the bottleneck is cleared. In addition, the SDEV of the densities rapidly increases to the maximum value just before

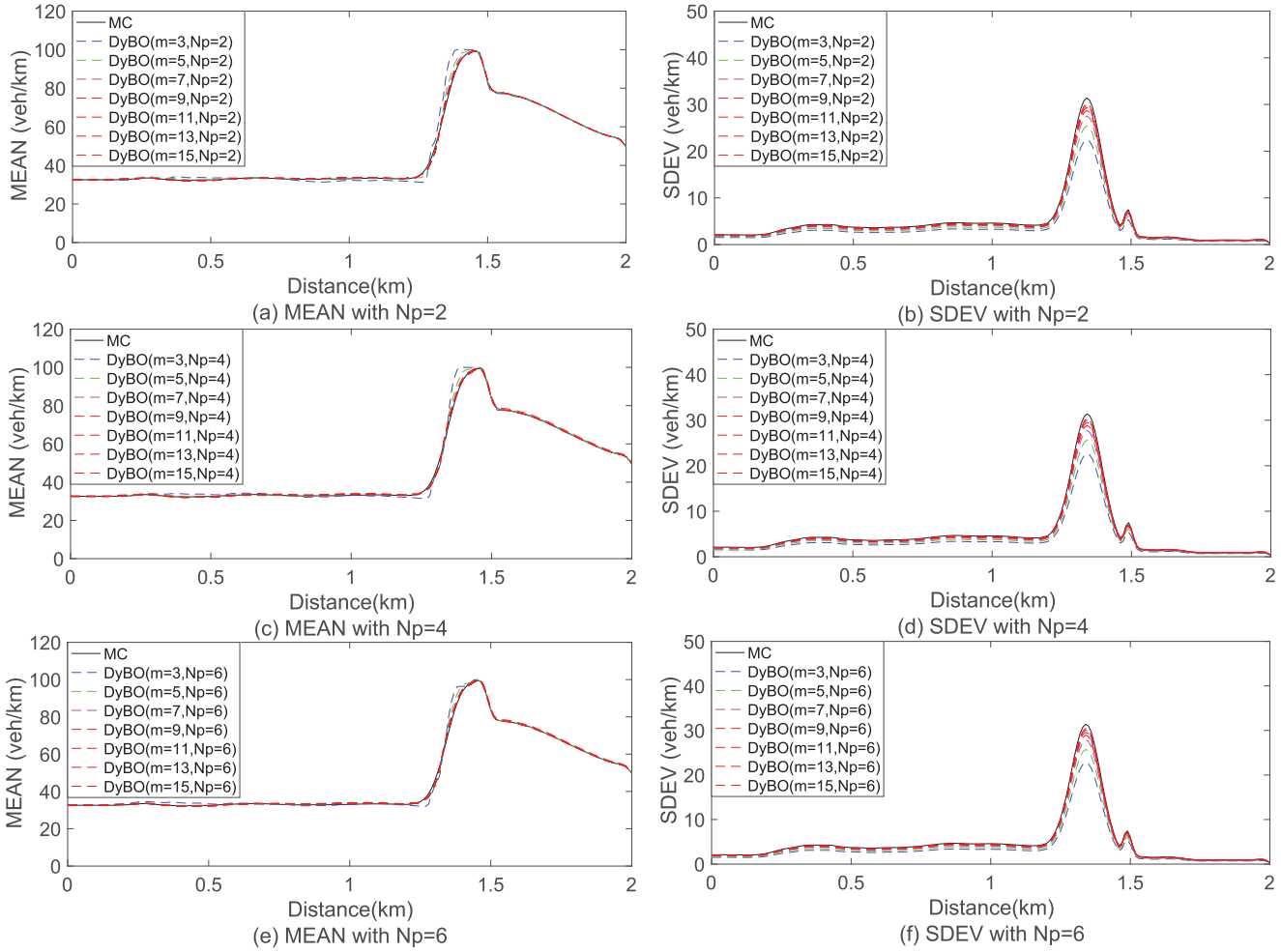

FIGURE 6 Density patterns at $t = 0.78$ h. DyBO, dynamically bi-orthogonal; MC, Monte Carlo; MEAN, mean; SDEV, standard deviation

the jam density is reached; it then significantly drops and then climbs again to the optimal density. This reflects the large variation in density at the start of a queue, which is commonly observed in daily traffic. Additionally, as more vehicles are fully stopped at the jam density, the variation in speeds decreases.

The above queuing phenomena can be observed throughout the road section at a given point in time (see Figure 11). The SDEV of the densities is smaller and more stable in the free-flow region than in a congested region. The SDEV of the densities becomes smaller and more stable when discharging because traffic dynamics can vary considerably across different compositions of drivers in the stop-and-go condition but remain basically the same during the completely stopped condition. In addition, as shown by the fundamental diagram, shockwave speeds decrease with increasing densities in the free-flow condition, but increase with increasing densities in the oversaturated condition. Therefore, an increase in the heterogeneity of the driver population increases the variations in traffic dynamics.

As the discontinuity of the traffic flow is caused by a bottleneck, a capacity drop phenomenon is expected as has long been commonly observed in empirical data (Geroliminis & Sun, 2011). This suggests that the queue discharge rate is lower than the pre-queue capacity. As shown in Figure 12, the traffic flow increases from zero in the free-flow condition to capacity in the congested condition (blue dots), and then drops to zero at the jam density. From congested condition to the free-flow condition (orange dots), traffic flow increases from zero to the discharge rate, and then drops back to a stable density that is significantly lower than the pre-queue capacity. The mean of the discharge density is 1676 veh/h, which is around 4% lower than the pre-queue capacity. The standard deviation of the discharge rate is 54 veh/h. This high standard deviation is attributable to the heterogeneity of the drivers' speeds in the discharging flow, and is consistent with the previous finding that the magnitude of capacity drops is variable. The vehicles' speed in congestion appears to correlate well with the queue discharge rate (Yuan et al., 2015).

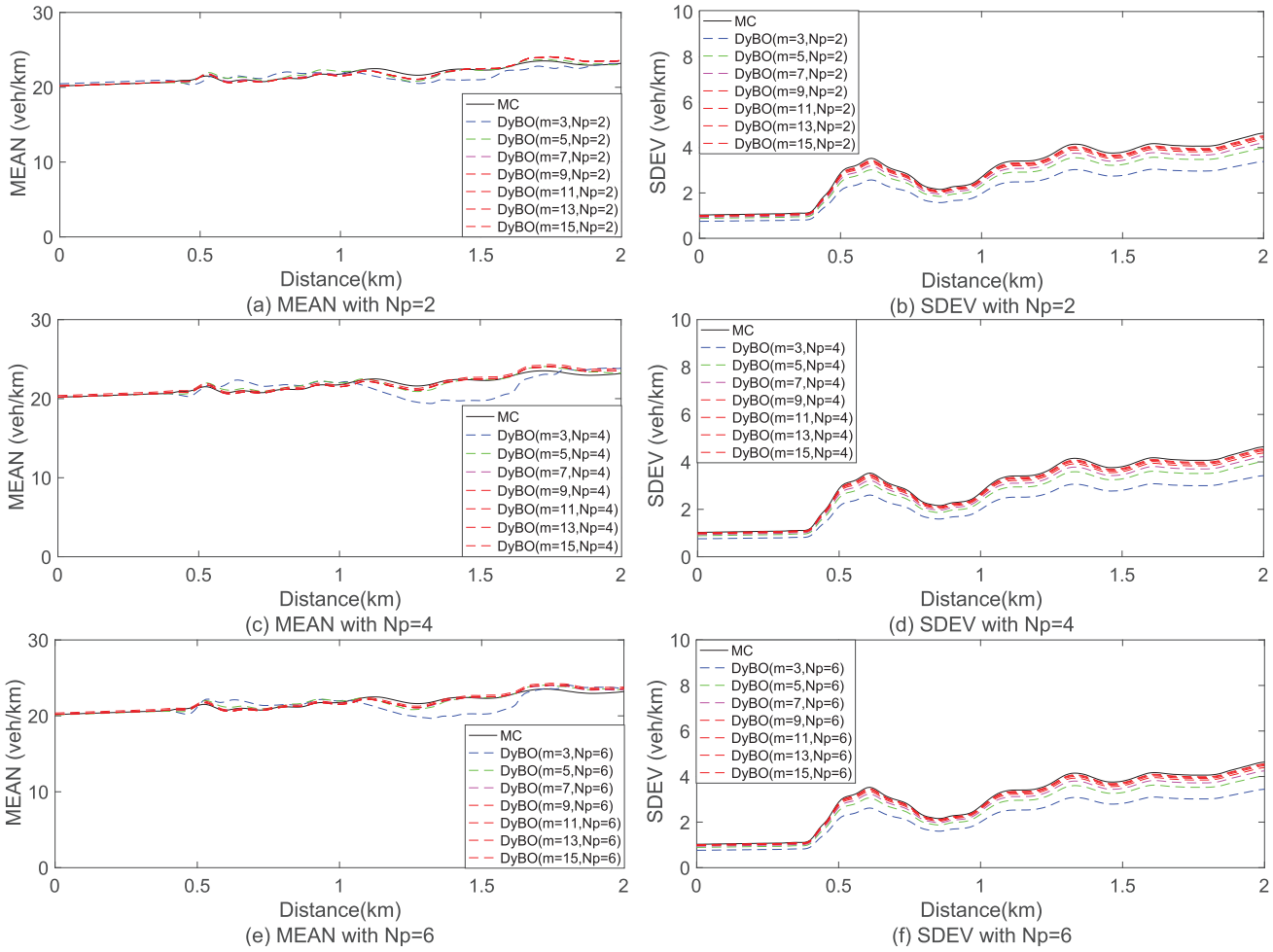

FIGURE 7 Density patterns at $t = 1.2$ h. DyBO, dynamically bi-orthogonal; MC, Monte Carlo; MEAN, mean; SDEV, standard deviation

TABLE 1 Relative root-mean-squared error of statistical quantities computed by the dynamically bi-orthogonal and Monte Carlo methods

	No. of Hermite polynomials: $N_p = 2$			No. of Hermite polynomials: $N_p = 4$			No. of Hermite polynomials: $N_p = 6$		
No. of spatial basis	Mean (MEAN)	Standard deviation (SDEV)	Time (min)	MEAN	SDEV	Time (min)	MEAN	SDEV	Time (min)
$m = 3$	5.1%	24.5%	1.74	4.2%	23.6%	1.77	3.8%	23.0%	1.82
$m = 5$	2.2%	13.6%	1.79	2.0%	12.7%	1.81	2.0%	12.2%	1.85
$m = 7$	1.2%	8.0%	1.82	1.1%	7.3%	1.83	1.0%	6.7%	1.89
$m = 9$	0.7%	4.4%	1.85	0.6%	3.9%	1.85	0.5%	3.5%	1.93
$m = 11$	0.5%	3.1%	1.87	0.3%	2.4%	1.90	0.3%	2.0%	1.99
$m = 13$	0.4%	2.4%	1.89	0.2%	1.4%	1.94	0.2%	1.2%	2.03
$m = 15$	0.2%	1.7%	1.93	0.2%	1.0%	1.96	0.2%	0.9%	2.08

4.2 | Example 2

4.2.1 | Example settings

As shown in Table 2, a 6-km heterogeneous highway with two geometric bottlenecks, represented by the jam density, was considered. Other settings remained the same as the first example except that the simulation period was 2 h to observe queue dissipation at the downstream end.

4.2.2 | Numerical results

To achieve an acceptable level of accuracy where RRMSE of both MEAN and SDEV are all below 5%, the numbers

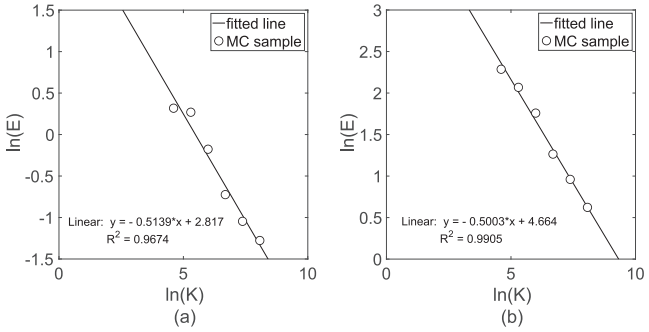

FIGURE 8 Relationship between the number of MC samples and errors of the MC method: (a) MEAN and (b) SDEV

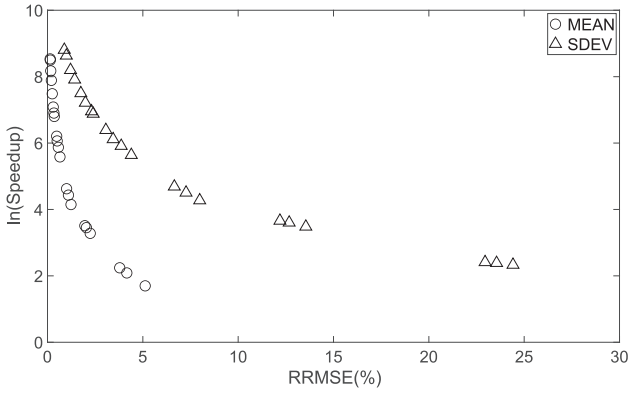

FIGURE 9 Relationship between speedup and RRMSE

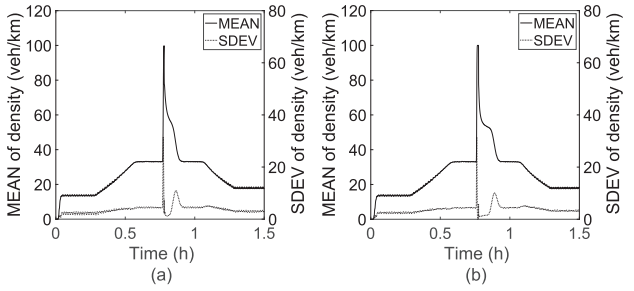

FIGURE 10 Density patterns at different locations: (a) $x = 1.5$ km; (b) $x = 1.75$ km

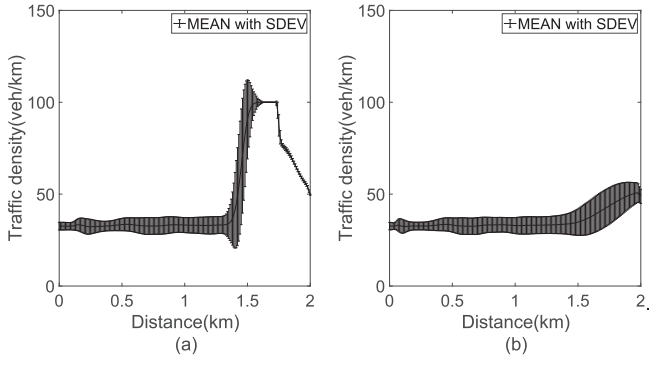

FIGURE 11 Density patterns at different times: (a) $t = 0.77$ h; (b) $t = 0.88$ h

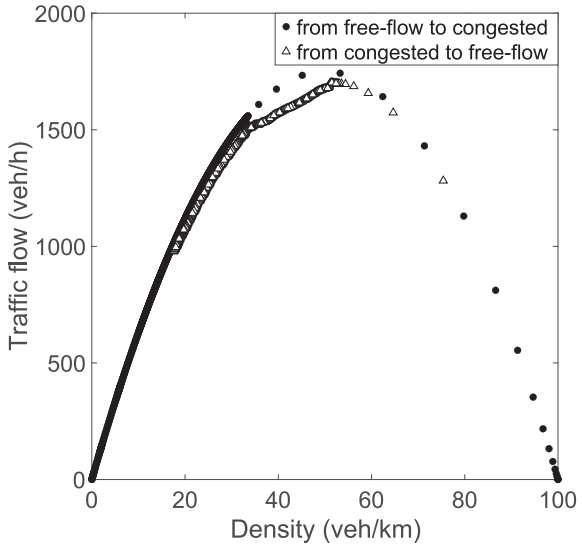

FIGURE 12 Capacity drop observed at the end of the road section

of spatial terms and Hermite polynomials were selected as $m = 9$, and $N_p = 4$. In addition, MC solutions with 1000 MC samples were presented for comparison. The computation times for the DyBO method and the MC method were 5.6 and 2841 min, respectively.

Road Sections 2 and 4 have lower jam densities, thereby lower capacities. As the traffic demand increases beyond their capacities, queues are formed expectedly. With no blockage at the end of the road section, the queues should gradually discharge and clear up eventually as long as the traffic demand remains below capacity. Typical time slots are selected to show how the density evolves along this heterogeneous highway.

As shown in Figure 13, at $t = 0.3$ h, traffic demand was lower than capacities of all the road sections, and hence no queue was formed, but the MEAN of Road Sections 2 and 4 were slightly higher than those of Road Sections 1 and 3 due to lower jam densities. Afterward, at $t = 0.8$ h, two queues were formed at the beginning of Road Sections 2 and 4, which were propagated upstream because traffic demand was beyond capacities of Road Sections 2 and 4. The MEAN of the downstream queue was a slightly higher than that of the upstream queue because of lower jam density. These two queues were discharging at their optimal densities, that is, 40 veh/km and 35 veh/km, respectively. When the traffic demand remained above the capacities of bottlenecks, the queues continue to grow. At $t = 1.2$ h, the MEAN of Road Section 2 was beyond 40 veh/km (the optimal density), indicating that it was in the congested state. This is because the downstream queue was spilled back to Road Section 2. When the traffic demand was lower than capacities of bottlenecks, the queue length began to decrease. At $t = 2$ h, only the downstream queue existed

TABLE 2 Jam densities of different road sections

Road section	Length (km)	Jam density (veh/km)	Description
1	0–3	100	Long enough to hold the queuing vehicles
2	3–4	80	With a capacity drop
3	4–5	100	Same setting as Road Section 1
4	5–6	70	Second bottleneck with further capacity drop to show the second queue at the downstream end

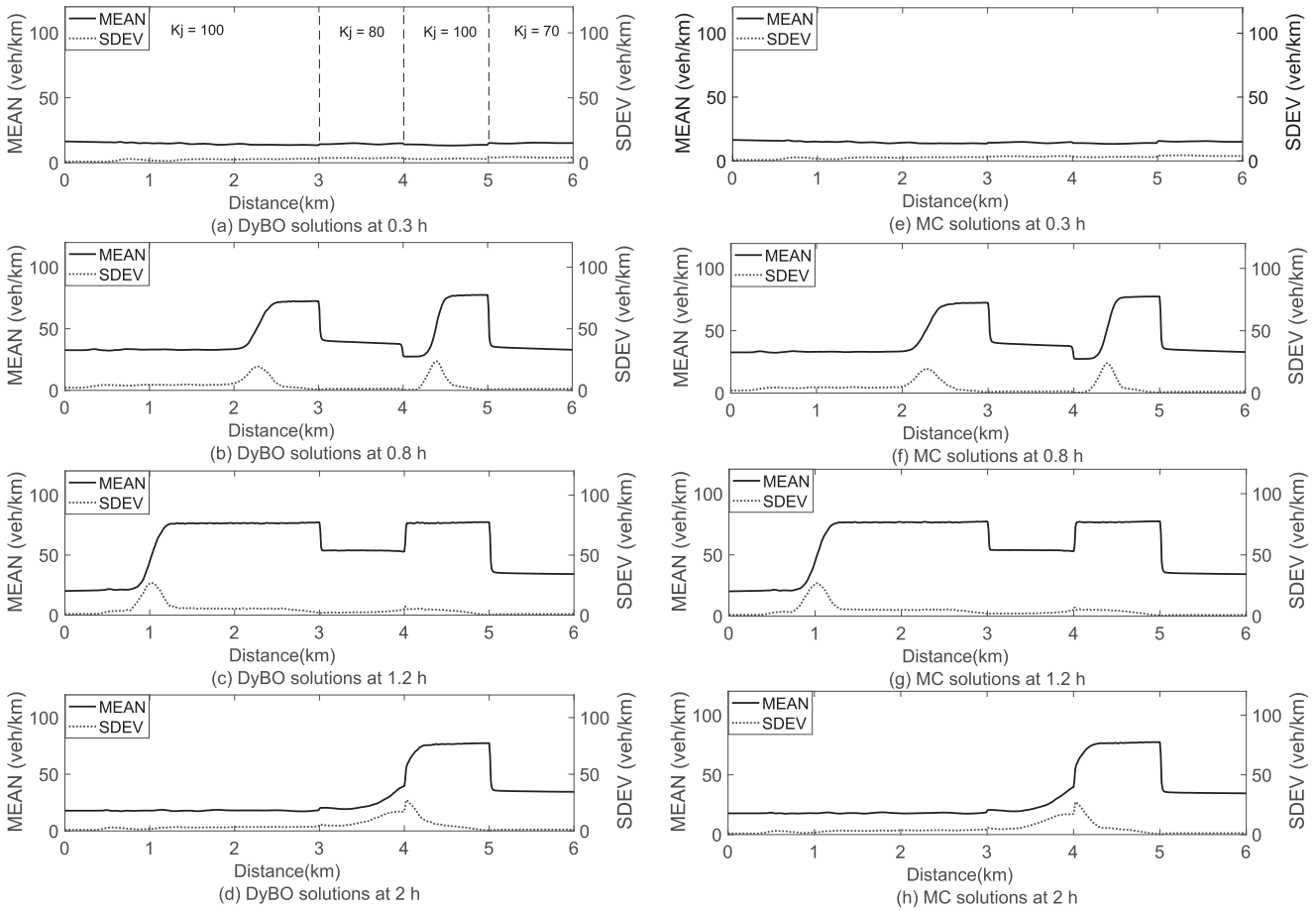

FIGURE 13 Density patterns with geometric bottlenecks (left column: dynamically bi-orthogonal [DyBO] solutions; right column: MC solutions)

and was discharging at the optimal density (35 veh/km). The upstream flow was in the free-flow state, and hence the downstream queue was expected to clear eventually.

Based on these density patterns, this experiment well demonstrated the good performance of the DyBO method in solving the SLWR model with geometric bottlenecks.

5 | CONCLUSION

This paper developed a new framework for examining the stochasticity in macroscopic traffic flow modeling, under which the free-flow speed is randomized to represent the heterogeneity in a driver population. Individual drivers are allowed to maintain consistent and rational behavior along the road section, which differentiates this framework from previous studies and makes model formulation more challenging. In the first example, stochastic variabilities were observed across the roadway section over time, and the MEAN and SDEV of traffic dynamics were calculated. In addition, some commonly observed traffic phenomena, including capacity drop, were reproduced. In the second example, the proposed model was shown to be well adaptative to heterogeneous road sections. In contrast to the

classic LWR model, the proposed model can help users to explore the stochastic paradigm, which may be useful in traffic planning, design, and real-time management. For example, if the stochastic speed paradigm is known, it will be feasible to use variable speed limit signs to actively manage real-time traffic operations.

Furthermore, the DyBO method was applied to improve the efficiency of solving the highly non-linear SPDE, and a sensitivity analysis of the DyBO method was conducted under various settings. Compared with the MC method, the DyBO method significantly decreased the computation time while maintaining desirable accuracy, thereby making it suitable for engineering practice. For example, in practical road network design problems, the evaluation model must be updated every time the network conditions change, and it is very computationally expensive to consider stochasticity in evaluation models. Our study shows that the DyBO method can substantially decrease computational burdens. In practice, there are many sources of stochasticity. As this paper is the first attempt to develop an SLWR model under the assumption of a stochastic source and to implement the DyBO method, it has some limitations that should be addressed in future research. For example, multiple random parameters could be included, and real-traffic data could be collected to test the proposed model.

ACKNOWLEDGMENTS

The first author was supported by a Postgraduate Scholarship from the University of Hong Kong. The second author was supported by the Research Grants Council of the Hong Kong Special Administrative Region, China (Project Nos.: 17204919 and R5029-18) and Francis S Y Bong Professorship in Engineering. The third author was supported by the Research Grants Council of the Hong Kong Special Administrative Region, China (Project Nos.: 17300318 and 17307921). The fourth author was supported by the National Natural Science Foundation of China (Project No.: NSFC 11801302) and the Tsinghua University Initiative Scientific Research Program.

REFERENCES

Adeli, H., & Ghosh-Dastidar, S. (2004). Mesoscopic-wavelet freeway work zone flow and congestion feature extraction model. *Journal of Transportation Engineering*, *130*(1), 94–103.

Babaee, H., Choi, M., Sapsis, T. P., & Karniadakis, G. E. (2017). A robust bi-orthogonal/dynamically-orthogonal method using the covariance pseudo-inverse with application to stochastic flow problems. *Journal of Computational Physics*, *344*, 303–319.

Babuška, I., Nobile, F., & Tempone, R. (2007). A stochastic collocation method for elliptic partial differential equations with random input data. *SIAM Journal on Numerical Analysis*, *45*(3), 1005–1034.

Cassidy, M. J., & Windover, J. R. (1995). Methodology for assessing dynamics of freeway traffic flow. *Transportation Research Record*, *1484*, 73–79.

Cheng, M., Hou, T. Y., & Zhang, Z. (2013a). A dynamically bi-orthogonal method for time-dependent stochastic partial differential equations I: Derivation and algorithms. *Journal of Computational Physics*, *242*, 843–868.

Cheng, M., Hou, T. Y., & Zhang, Z. (2013b). A dynamically bi-orthogonal method for time-dependent stochastic partial differential equations II: Adaptivity and generalizations. *Journal of Computational Physics*, *242*, 753–776.

Choi, M., Sapsis, T. P., & Em, G. (2014). On the equivalence of dynamically orthogonal and bi-orthogonal methods: Theory and numerical simulations. *Journal of Computational Physics*, *270*, 1–20.

Gazis, D. C., & Knapp, C. H. (1971). On-line estimation of traffic densities from time-series of flow and speed data. *Transportation Science*, *5*(3), 283–301.

Gazis, D., & Liu, C. (2003). Kalman filtering estimation of traffic counts for two network links in tandem. *Transportation Research. Part B*, *37*(8), 737–745.

Geroliminis, N., & Sun, J. (2011). Hysteresis phenomena of a macroscopic fundamental diagram in freeway networks. *Procedia–Social and Behavioral Sciences*, *17*, 213–228.

Ghosh-Dastidar, S., & Adeli, H. (2006). Neural network-wavelet microsimulation model for delay and queue length estimation at freeway work zones. *Journal of Transportation Engineering*, *132*(4), 331–341.

Giles, M. B. (2008). Multilevel Monte Carlo path simulation. *Operations Research*, *56*(3), 607–617.

Jabari, S. E., & Liu, H. X. (2012). A stochastic model of traffic flow: Theoretical foundations. *Transportation Research Part B*, *46*(1), 156–174.

Jahani, E., Muhanna, R. L., Shayanfar, M. A., & Barkhordari, M. A. (2014). Reliability assessment with fuzzy random variables using interval Monte Carlo simulation. *Computer-Aided Civil and Infrastructure Engineering*, *29*(3), 208–220.

Jiang, G. -S., & Shu, C. -W. (1996). Efficient implementation of weighted ENO schemes. *Journal of Computational Physics*, *126*(1), 202–228.

Li, J., Chen, Q. -Y., Wang, H., & Ni, D. (2012). Analysis of LWR model with fundamental diagram subject to uncertainties. *Transportmetrica*, *8*(6), 387–405.

Lighthill, M. J., & Whitham, G. B. (1955). On kinematic waves. II. A Theory of traffic flow on long crowded roads. *Proceedings of the Royal Society of London. Series A, Mathematical and Physical Sciences*, *229*(1178), 317–345.

Martínez, I., & Jin, W. L. (2020). Stochastic LWR model with heterogeneous vehicles: Theory and application for autonomous vehicles. *Transportation Research Procedia*, *47*, 155–162.

Newman, A. J. (1996a). *Model reduction via the Karhunen-Loeve expansion Part I: An exposition*. Technical Report T.R.96-32, Institute for Systems Research, University of Maryland, Maryland.

Newman, A. J. (1996b). *Model reduction via the Karhunen-Loeve expansion Part II: Some elementary examples*. Technical Report T.R.96-32, Institute for Systems Research, University of Maryland, Maryland.

Prigogine, I., & Herman, R. (1971). *Kinetic theory of vehicular traffic*. Elsevier.

Richards, P. I. (1956). Shock waves on the highway. *Operations Research*, *4*(1), 42–51.

Shu, C. -W. (2020). Essentially non-oscillatory and weighted essentially non-oscillatory schemes. *Acta Numerica*, *29*, 701–762.

Shu, C. -W. (2006). Essentially non-oscillatory and weighted essentially non-oscillatory schemes for hyperbolic conservation laws. In A. Quarteroni (Ed.), *Advanced numerical approximation of nonlinear hyperbolic equations* (pp. 325–432). Springer.

Sumalee, A., Zhong, R. X., Pan, T. L., & Szeto, W. Y. (2011). Stochastic cell transmission model (SCTM): A stochastic dynamic traffic model for traffic state surveillance and assignment. *Transportation Research Part B*, *45*(3), 507–533.

Szeto, W. Y., Jiang, Y., & Sumalee, A. (2011). A cell-based model for multi-class doubly stochastic dynamic traffic assignment. *Computer-Aided Civil and Infrastructure Engineering*, *26*(8), 595–611.

Wan, X., & Karniadakis, G. E. M. (2006). Multi-element generalized polynomial chaos for arbitrary probability measures. *SIAM Journal on Scientific Computing*, *28*(3), 901–928.

Xiong, T., Zhang, M., Shu, C. W., Wong, S. C., & Zhang, P. (2011). High-order computational scheme for a dynamic continuum model for bi-directional pedestrian flows. *Computer-Aided Civil and Infrastructure Engineering*, *26*(4), 298–310.

Xiu, D., & Em Karniadakis, G. (2003). The Wiener-Askey polynomial chaos for stochastic differential equations. *SIAM Journal on Scientific Computing*, *24*(2), 619–644.

Xiu, D., Lucor, D., Su, C. -H., & Karniadakis, G. E. (2002). Stochastic modeling of flow-structure interactions using generalized polynomial chaos. *Journal of Fluids Engineering*, *124*(1), 51–59.

Yuan, K., Knoop, V. L., & Hoogendoorn, S. P. (2015). Capacity drop: Relationship between speed in congestion and the queue discharge rate. *Transportation Research Record*, *2491*, 72–80.

Zhang, M., Shu, C. W., Wong, G. C. K., & Wong, S. C. (2003). A weighted essentially non-oscillatory numerical scheme for a multi-class Lighthill-Whitham-Richards traffic flow model. *Journal of Computational Physics*, *191*(2), 639–659.

Zheng, Z. (2021). Reasons, challenges, and some tools for doing reproducible transportation research. *Communications in Transportation Research*, *1*, 100004.

Zhou, B., Bliemer, M. C. J., Bell, M. G. H., & He, J. (2016). Two new methods for solving the path-based stochastic user equilibrium problem. *Computer-Aided Civil and Infrastructure Engineering*, *31*(2), 100–116.

How to cite this article: Fan, T., Wong, S. C., Zhang, Z., & Du, J. (2023). A dynamically bi-orthogonal solution method for a stochastic Lighthill-Whitham-Richards traffic flow model. *Computer-Aided Civil and Infrastructure Engineering*, *38,* 1447–1461. https://doi.org/10.1111/mice.12953